ACS Sustainable Chemistry & Engineering

Research Article

pubs.acs.org/journal/ascecg

Iron Oxide with Facilitated O^{2-} Transport for Facile Fuel Oxidation and CO_2 Capture in a Chemical Looping Scheme

Nathan L. Galinsky, Yan Huang, Arya Shafiefarhood, and Fanxing Li*

Department of Chemical and Biomolecular Engineering, North Carolina State University, 911 Partners Way, Raleigh, North Carolina 27695-7905, United States

Supporting Information

ABSTRACT: The chemical looping strategy offers a potentially viable option for efficient carbonaceous fuel conversion with a reduced carbon footprint. In the chemical looping process, an oxygen carrier is reduced and oxidized in a cyclic manner to convert a carbonaceous fuel into separate streams of concentrated carbon dioxide and carbon-free products such as electricity and/or hydrogen. The reactivity and chemical and physical stability of the oxygen carrier are of pivotal importance to chemical looping processes. A typical oxygen carrier is composed of a multi-valence transition metal oxide supported on an "inert" support. Although the support does not get reduced or oxidized at any significant extent, numerous studies have indicated that certain supports such as TiO_2 and Al_2O_3 can improve oxygen carrier stability and/or reactivity. This study reports the use of mixed ionic−electronic conductive support in iron-based oxygen carriers. By incorporating a perovskite-based mixed conductive support such as lanthanum strontium ferrite (LSF), the reactivity of the oxygen carrier is enhanced by 5−70 times when compared to oxygen carriers with conventional TiO_2-, Al_2O_3-, or yttria-stabilized zirconia (YSZ) support. The mixed conductivity enhanced oxygen carrier also shows good stability and coke resistance. Characterization studies indicate that the enhanced oxygen carrier is composed of intermixed nanoscale (<100 nm) crystallites of iron oxide and support. The mixed conductive support enables facile O^{2-} transport to and from the iron oxide nanocrystallites to participate in the surface redox reactions. The support also allows counter-current or concurrent diffusion of electrons or holes to maintain charge balance within the oxygen carrier. With iron oxide as the nanoscale oxygen source and mixed conductive support as the oxygen/electron conductor, the mixed conductivity enhanced oxygen carrier particle can be considered as an ensemble of nanoscale mixed conductive membrane reactors that possess excellent redox activity.

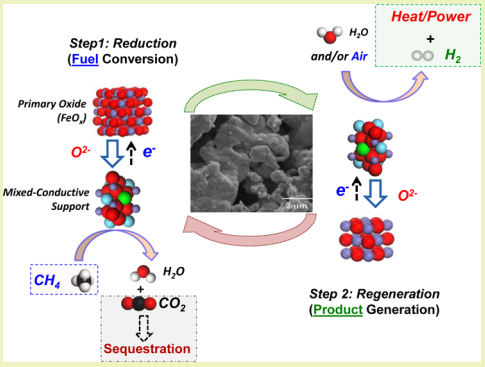

KEYWORDS: *CO_2 capture, Oxygen carrier, Chemical looping*

INTRODUCTION

The chemical looping strategy represents a unique alternative to conventional combustion- or gasification-based approaches for power and/or hydrogen generation from carbonaceous fuels.[1−6] In chemical looping processes, carbonaceous fuels are converted by an oxygen carrier particle in two or more reduction and oxidation (redox) steps. These redox steps allow the oxygen carrier to shuttle oxygen from oxidants such as air or steam to the fuel in a cyclic manner. During the reduction step, the oxygen carrier donates oxygen to the fuel, resulting in a gaseous mixture with concentrated carbon dioxide and water vapor. The oxygen-deprived oxygen carrier is then replenished in the regeneration or oxidation step(s) in which heat and/or hydrogen is produced.[1−3,7−11] Simplified reactions in the reduction and regenerations steps are given below

$$\text{Reduction Step:}\quad C_xH_y(\text{Fuel}) + MeO_m(\text{oxygen carrier}) \leftrightarrow MeO_{m-n} + y/2H_2O + xCO_2$$

$$\text{Regeneration Step:}\quad MeO_{m-n}(\text{oxygen carrier}) + H_2O/O_2 \leftrightarrow MeO_m + H_2/\text{Heat}(\text{products})$$

Because the oxygen carrier is essential to key chemical looping reactions, its selection and optimization are of utmost importance to the novel chemical looping process.

An oxygen carrier is typically composed of a primary metal oxide and a support.[7,12−14] The primary metal oxide, often composed of oxides of iron, nickel, copper, manganese, and/or cobalt, functions as the active redox material for oxygen storage and donation purposes.[7,12,15] The support, on the other hand, usually does not directly participate in chemical looping reactions. The presence of support is found to improve the

Received: December 26, 2012
Revised: January 30, 2013
Published: February 2, 2013

reactivity and/or long-term stability of the oxygen carrier.[1] Besides supported transition metal oxides, mixed metal oxide-based oxygen carriers such as iron-containing perovskites and mixed Mn and Fe oxides are also investigated as potential oxygen carrier candidates for chemical looping applications.[16−19] Although mixed metal oxides of Mn and Fe showed promising properties for chemical looping with oxygen uncoupling, they do not possess the thermodynamic properties required for hydrogen generation.[10,20] Perovskite materials, although potentially feasible for hydrogen generation,[17,21] generally exhibit a low oxygen transport capacity.[4,16,17] Because of the lack of oxygen storage and donation capabilities, fuel conversion using perovskite-based oxygen carriers is often limited.[4,16,17,22] The selection criteria for oxygen carriers have been discussed in a number of previous publications.[7,12,15] A rational strategy for oxygen carrier design and optimization, however, has yet to be developed because (i) oxygen carrier design can be a challenging task considering the many desired physical and chemical properties, and (ii) there is a lack of fundamental understanding of the roles of the primary metal oxide, support, and their interactions. To date, more than 700 oxygen carriers obtained from various metal oxide support combinations and synthesis techniques have been reported.[1] A trial and error type of approach is often adopted in these studies. In an attempt to further understand the redox scheme of iron-based oxygen carriers, Li et al. recently investigated the effect of TiO_2 support on the reactivity of iron oxide-based oxygen carriers. Using both experiment and ab initio calculation tools, they demonstrated that TiO_2 support lowers the activation energy for oxygen anion (O^{2-}) transfer through the metal oxide lattice.[23,24] The lowered activation energy for O^{2-} conduction and substitution defects of O^{2-} created by support addition are considered to be the key contributors to the enhanced oxygen carrier performance after support addition.

In this article, we attempt to rationalize the design strategy of iron-based oxygen carriers by incorporating mixed ionic−electronic conductive (MIEC) support. It is proposed that the MIEC support facilitates countercurrent conduction of O^{2-} and electrons, thereby allowing facile O^{2-} transport to and from the iron oxide irrespective to the porosity of the oxygen carrier particle. Although TiO_2-supported Fe_2O_3 is considered as an active oxygen carrier in previous research,[1,15] the present study indicates that more than 1 order of magnitude reactivity improvement for methane conversion can be achieved by replacing the TiO_2 with an MIEC support such as $La_{0.8}Sr_{0.2}FeO_{3-\delta}$ (LSF). The use of LSF support instead of conventional TiO_2-based support has also led to 5−70 fold reactivity enhancements in oxygen carrier reactivity for converting a variety of fuels including H_2, CO, and CH_4. The LSF-supported iron oxide exhibits excellent activity at a low temperature of 450 °C, which is 250 °C lower than the initial reduction temperature of the TiO_2-supported oxygen carrier. The stability of the LSF-supported oxygen carrier is confirmed by a 50 cycle continuous redox experiment, which indicates stable phase composition, near constant crystalline sizes, and minimal decrease in reactivity. Coke formation is found to be minimal in all cases. Compared to oxygen carriers with other commonly used supports such as Al_2O_3 and YSZ, LSF-supported Fe_2O_3 is also significantly more active. Scanning electron microscope (SEM), energy dispersive X-ray spectroscopy (EDX), and X-ray photoelectron spectroscopy (XPS) studies reveal that the oxygen carrier particles are composed of micrometer-sized dense grains. Each grain can be considered as an interpenetrated matrix of nanoscale LSF support and iron oxide crystallites. Although oxygen conductivity in iron oxides tends to be low, the nanoscale interaction between the MIEC support and iron oxide creates a solid-state O^{2-} and electron/hole pathway that allows full accessibility of active oxygen in iron oxide, even at a low surface area. The present study validates that MIEC support can significantly enhance the reactivity of iron oxide-based oxygen carriers. Because a key limitation of iron oxide-based oxygen carriers is their low reactivity,[7,12,13,25] the MIEC-supported oxygen carrier developed in the present study can potentially be effective for chemical looping combustion and gasification applications.

EXPERIMENTAL SECTION

Oxygen Carrier Synthesis. Fe_2O_3 supported with TiO_2 and $La_{0.8}Sr_{0.2}FeO_3$, both with 60 wt % Fe_2O_3 loading, are prepared. TiO_2-supported Fe_2O_3 is used as a reference oxygen carrier because TiO_2-supported iron oxide and ilmenite are frequently studied oxygen carriers with satisfactory reactivity.[26−31] A simple "one pot" solid state reaction (SSR) method is used for oxygen carrier synthesis. The general procedure involves preparation of a powder mixture followed by pelletization and annealing/solid-state reaction. To prepare Fe_2O_3-supported TiO_2 particles, calculated amounts of TiO_2 (99.9%, Noah Chemicals) and Fe_2O_3 (99.9%, Noah chemicals) precursors are mixed for 1 h in a planetary ball mill (XBM4X, Columbia International) at a rotation speed of 250 rpm. The mixture is then pressed into pellets by a hydraulic press (YLJ-15T, MTI Corporation) at the pressure of 6 MPa and sintered in a high temperature tube Furnace (GSL-1500-X50, MTI Corporation) at 1200 °C for 8 h. Samples of Al_2O_3- (99% pure, Noah Chemical) and YSZ- (99% pure, Noah Chemical) supported Fe_2O_3 are also prepared using the method identical to the TiO_2-supported Fe_2O_3. Sintering time of 28 h at 1200 °C was used to ensure comparable surface areas among the various oxygen carrier samples. Pure iron oxide, sintered for 8 h, is also tested. The Fe_2O_3/$La_{0.8}Sr_{0.2}FeO_3$ particles are prepared by mixing calculated amounts of La_2O_3 (99.9%, Aldrich), $SrCO_3$ (99.9%, Noah Chemical), and Fe_2O_3 precursors for 3 h in the planetary ball mill at a rotation speed of 250 rpm. The mixed powder is then pressed and sintered at 1200 °C. Two samples, one sintered for 8 h and the other for 28 h, were prepared for comparison purpose. High pelletization pressure and sintering temperature are used to ensure sufficient solid-state reaction and to obtain particles with comparable (low) porosity. The sintered pellets are finally fractured and sieved to arrive at particulates of various size ranges. Particles of 150−250 μm in size are used in all the reactivity studies because such a size range is suitable for chemical looping operations in a circulating fluidized bed reactor.[32,33]

Reactivity Studies. All the reactivity studies are conducted in a SETARAM SETSYS Evolution Thermal Gravimetric Analyzer (TGA). Initial studies are performed to determine the flow rate at which external mass transfer resistances are eliminated. This flow rate is determined by performing reduction experiments with a varying reducing gas flow rate, while keeping reaction temperature (900 °C) and reducing gas composition (10% H_2 balanced with He/N_2) constant. The relationship between the reducing gas flow rate and oxygen carrier reduction rate is recorded. At low gas flow rates, an increase in total gas flow rate generally leads to a higher oxygen carrier−H_2 reaction rate. The external mass transfer limitations are considered to be minimal when no further rate enhancement is observed with an increase in total gas velocity. Our experiments indicate that a total flow rate of 250 mL/min is adequate for eliminating the external mass transfer resistance. This corresponds to a linear gas velocity of approximately 1.2 m/s. Unless specified otherwise, the experiments are conducted at 900 °C with a sample weight of approximately 20 mg. The total gas flow rate is maintained at around 300 mL/min.

Three sets of redox experiments are conducted for both TiO_2-supported and LSF-supported oxygen carriers using hydrogen as the

reducing gas. These experiments include one cycle reduction−oxidation (redox), five cycle redox, and fifty cycle redox. The one cycle test provides information on initial redox activity of the oxygen carrier, whereas the five and fifty cycle experiments determine short and long-term recyclability of the oxygen carriers, respectively. The experimental conditions for these experiments are listed in Table 1.

Table 1. Experimental Conditions for 1 Cycle, 5 Cycle, and 50 Cycle Redox Experiments Using Hydrogen as the Reducing Gas

test	sample weight (mg)	reducing gas composition	oxidizing gas composition
1 cycle	20	10.5% H_2	4.1% O_2
5 cycle	20	10.5% H_2	4.1% O_2
50 cycle[a]	30	10% H_2	10% O_2

[a]The 50 cycle experiment is carried out to determine particle stability under redox conditions; 30 mg of sample is used to obtain an adequate sample for further characterizations. A higher O_2 concentration is used for the 50 cycle test to reduce the cycle time.

To determine the redox contribution from the LSF support, pure $La_{0.8}Sr_{0.2}FeO_3$ is tested for 5 h in 10% H_2 at 900 °C. TiO_2 support can also be reduced by H_2 at high temperature; previous studies have indicated that the redox contribution from TiO_2 tends to be low,[23,34] especially at the initial stage of the reduction.

Besides hydrogen, CO and CH_4 are also used as the reducing gases to determine the activity of the oxygen carriers and their resistance toward carbon deposition. A total of 10% CH_4 or CO balanced with inert gases is used in all the reducing experiments. Carbon analysis is performed on the solid samples using a CHN Elemental Analyzer (Perkin-Elmer-2400). To determine the initial reduction temperature of the oxygen carriers, experiments are performed in the TGA on TiO_2- and LSF-supported oxygen carriers under a temperature ramping mode with 10% H_2. The starting and ending points of the temperature ramp are 100 and 900 °C, respectively, and the temperature ramping rate is 5 °C/min. A Quantachrome ChemBET Pulsar temperature programmed reduction/desorption (TPR/TPD) instrument is also used to determine the sample reducibility at various temperatures. A total of 5% hydrogen mixed with argon is used as the reducing gas. Temperature ramping during the TPR experiment is 2 °C/min.

Sample Characterizations. The surface area, crystal structure, and surface and bulk elemental compositions of the oxygen carriers are analyzed using a variety of characterization tools. An X-ray powder diffraction (XRD) test is carried out to analyze the crystal phase composition before and after reduction cycles. XRD patterns are recorded using a Rigaku SmartLab X-ray diffractometer with Cu Kα (λ = 0.1542) radiation operating at 40 kV and 44 mA. Scans are performed stepwise with 0.1° step size holding for 5 s at each step in a 20−80° angle range (2θ). The specific surface areas of the samples are measured with a BET surface analyzer (Quantachrome QuadraSorb Station 1) using krypton or nitrogen physisorption at 77.3 K. Scanning electron microscopy (SEM, Hitachi S3200) is used to observe the surface morphology and structure of the samples. An accelerating voltage of 5−20 kV is used for image capture. The same instrument is used for elemental analysis of the samples using energy dispersive X-ray spectroscopy (EDX) technique. Both the surface and cross section of the oxygen carriers are examined using both EDX line scan and spot analysis (10 kV). The surface compositions of the oxygen carrier are also analyzed using X-ray photoelectron spectroscopy (XPS, SPECS-XPS) with an Mg Kα excitation (1254 eV) and a PHOIBIS 150 hemispherical analyzer at 10^{-10} mbar pressure. Energy calibration for the XPS is established by referencing to adventitious carbon (C1s line at 285.0 eV binding energy).

RESULTS AND DISCUSSION

In order to achieve smooth operation of chemical looping processes, oxygen carriers are processed into particulates of 100 μm or larger.[10] The interactions between oxygen carrier particles and gaseous reactants typically proceed via a number of steps including diffusion of reactants from bulk phase to sample surface, intraparticle gaseous diffusion, surface reactions, desorption and outward diffusion of the reaction products, etc.[1] Recent studies indicated that active oxygen in the oxygen carrier may also diffuse to its surface, via solid-state ionic conduction, to participate in the redox reactions.[15,23] In order to accurately evaluate the effect of mixed conductivity on the redox reactivity of the oxygen carrier, the contributions from external mass transfer resistances and intraparticle gaseous diffusion need to be isolated. As discussed in the Experimental section, external mass transfer resistance can be eliminated by performing the experiments at a high linear gas velocity. The effect of intraparticle gaseous diffusion can be offset by comparing oxygen carriers with similar porous structures but different mixed conductivities. As mentioned earlier, TiO_2-supported Fe_2O_3 is used as the reference oxygen carrier, whereas LSF-supported Fe_2O_3 is the oxygen carrier with improved mixed conductivity. In order to obtain oxygen carrier samples with comparable porous structure, a high sintering temperature of 1200 °C is used to eliminate most of the micropores and mesopores within the oxygen carrier particles. Surface analysis conducted using BET showed comparable low surface areas after sintering (Table S1, Supporting Information).

Reactivity with Hydrogen. The reaction between the oxygen carrier and fuels represents a key step in all chemical looping processes. Hydrogen is selected as the fuel for initial assessment of the oxygen carrier reactivity because no side reactions are likely to take place between hydrogen and the oxygen carrier samples. Therefore, reactivity with hydrogen can represent the "intrinsic" redox activity of the oxygen carrier. In addition, hydrogen is a commonly encountered fuel that is present in synthesis gas derived from various carbonaceous feedstocks. The TGA curves for oxygen carrier reduction with 10.5% H_2 are illustrated in Figure 1. The TGA records the weight loss of the oxygen carrier during its reduction reactions. Because the weight loss of the solid sample directly corresponds

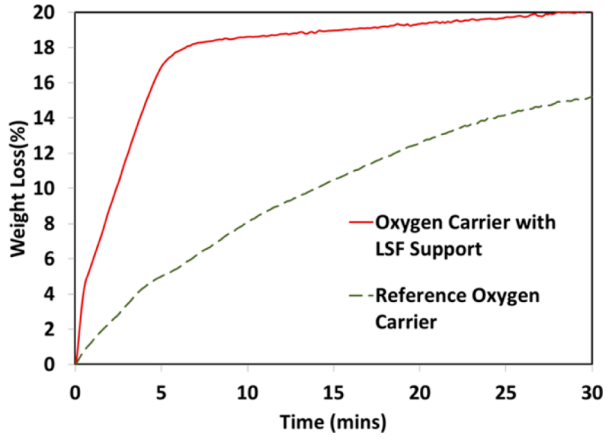

Figure 1. Reduction of as-prepared LSF- and TiO_2- supported iron oxide particles in a TGA apparatus (10% H_2 balanced with N_2/He, 900 °C. Reference oxygen carrier refers to TiO_2-supported iron oxide).

dx.doi.org/10.1021/sc300177j | ACS Sustainable Chem. Eng. 2013, 1, 364−373

to its extent of reduction, the points on the TGA curves in Figure 1 can be converted into oxygen carrier conversion via eq 1

$$\%\text{conversion} = \frac{(m_{\text{initial}} - m_i)}{m_{\text{initial}} \times x_{O2}} \times 100\% \quad (1)$$

where m_{initial} is the initial mass of the oxygen carrier, m_i is the mass at the time of interest during the reduction step, and x_{O2} is the weight percent of active oxygen in the unreacted oxygen carrier. In the current study, the support materials, i.e., TiO_2 or LSF, are considered as "inert", whereas all the oxygen atoms in Fe_2O_3 are considered active. Because 60% Fe_2O_3 is used in all the oxygen carriers, x_{O2} is ~18% in all cases. It should be noted that many previous studies only consider 11% of the oxygen in Fe_2O_3 as active oxygen ($Fe_2O_3 \leftrightarrow Fe_3O_4$). This is different from that in the present study which considers full reduction of Fe_2O_3 to Fe. It is also noted that both TiO_2 and LSF can be reduced at a high temperature under a hydrogen environment. The contribution of TiO_2 reduction to the overall reduction kinetics of the oxygen carrier; however, has been determined to be minimal.[23,34] Reduction experiments using pure LSF indicates that the contribution of LSF support to the oxygen carrier reduction kinetics is within 2% of the total conversion (Figure S1, Supporting Information). Therefore, LSF mainly functions as a redox reaction promoter as opposed to a reactant.

The reaction rates of the TiO_2-supported and LSF-supported iron oxide samples are compared using three quantitative parameters including the initial reaction rate, time required to reach 11% conversion, and time required to achieve 33% conversion. Initial reaction rate (%conversion/sec) reflects the intrinsic reactivity between the oxygen carrier surface region and reducing gas. The time required (min) to reach 11% and 33% conversions provides indication of the overall activity of the oxygen carrier. The 11% and 33% conversions correspond to iron oxide reduction to Fe_3O_4 and FeO, respectively. The rate comparisons for the oxygen carriers with the two different supports are shown in Figure 2. As shown, the initial rate of the LSF-supported oxygen carrier is approximately 5 times higher than that of the oxygen carrier with the TiO_2 support. To reach conversions of 11% and 33%, the TiO_2-supported oxygen carrier requires an approximately 6 times longer reaction time.

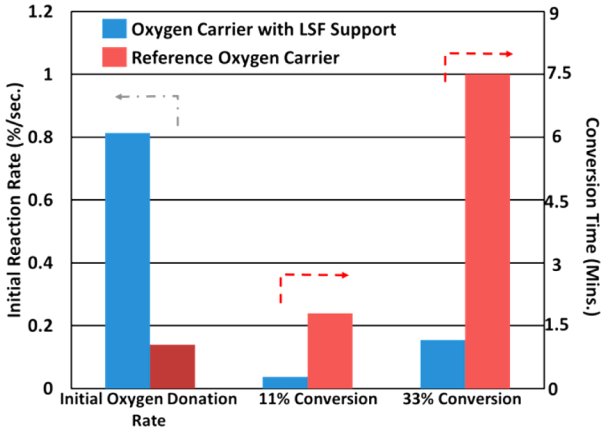

Figure 2. Reactivity comparisons of as-prepared TiO_2-supported Fe_2O_3 (reference oxygen carrier) and LSF-supported Fe_2O_3 (oxygen carrier with enhanced mixed conductivity). Reducing gas, 10.5% hydrogen; temperature, 900 °C.

Beyond 33% conversion, the reduction rate of the TiO_2-supported oxygen carrier slows down significantly faster than the LSF-supported oxygen carrier. As indicated in Figure 1, the LSF-supported oxygen carrier shows complete oxygen donation from iron oxide within a much shorter time frame, indicating that the active oxygen atoms in iron oxide can effectively react with hydrogen even at a very low surface area. The continued weight loss beyond 18 wt % oxygen donation mainly results from the slow reduction of the LSF support. To determine the temperature dependence of the oxygen carrier redox reactivity, the two aforementioned oxygen carriers are reduced in hydrogen under a temperature ramp in both TGA and TPR. As illustrated in Figure 3, the initial reduction temperature of the LSF-supported Fe_2O_3 is roughly 250 °C lower than TiO_2-supported Fe_2O_3. The significant decrease in initial reduction temperature further confirms the superior reactivity of the oxygen carrier enhanced by the mixed conductive support. The TPR results of TiO_2-supported Fe_2O_3 shown in Figure 3(b) are qualitatively consistent with those obtained by previous researchers on impregnated TiO_2–Fe_2O_3 oxygen carriers using 10% H_2 as the reducing gas.[26] In contrast, the LSF-supported Fe_2O_3 exhibits its major reduction peak at a temperature much lower than the typical reduction temperature of β-oxygen in LSF.[17] This is likely to result from the synergistic effect of LSF and Fe_2O_3 coupled with the relatively low reducible oxygen content in the LSF support.

Previous studies have indicated that ilmenite and TiO_2-supported iron oxide particles can be "activated" during the first few redox cycles due to their morphology and porosity change.[24,25] Figure 4 compares the reactivity of the TiO_2- and LSF-supported iron oxide over five redox cycles. Consistent with previous studies, the reactivity of the TiO_2-supported oxygen carrier significantly increases over the first three redox cycles and then stabilizes. To compare, reactivity of the LSF-supported oxygen carrier is much more stable. Even at the fifth cycle, the LSF-supported oxygen carrier is still five times more reactive than the TiO_2-supported oxygen carrier for hydrogen conversion. Reactivity studies on porous oxygen carriers obtained using starch template also indicate that the LSF-supported oxygen carrier is far more reactive than the oxygen carrier with the TiO_2 support (Figure S4, Supporting Information).

Long-Term Stability of the LSF-Supported Oxygen Carrier. The ability of an oxygen carrier to maintain high reactivity and phase stability over multiple redox cycles at high temperatures is highly desirable for chemical looping applications. With an LSF-supported oxygen carrier exhibiting promising reactivity, studies are carried out to investigate its long-term stability. The TGA curves of the LSF-supported oxygen carrier over 50 redox cycles are provided in Figure 5. As indicated in Figure 5, the LSF-supported oxygen carrier shows less than a 4% decay in reactivity for both reduction and oxidation reactions over the 50 redox cycles. During the experiment, iron oxide is reduced to iron phase in all reduction cycles. An insignificant extent of sintering is observed on the sample, as manifested by loose attachment of particulates. Sintering may account for the small loss in reactivity over multiple redox cycles. It is likely to result from the complete reduction of Fe_2O_3 to iron and subsequent combustion reaction. Combustion of metallic iron with oxygen is highly exothermic and can lead to melting of iron, which has a much lower melting point than iron oxides. Sintering can be completely avoidable in actual chemical looping combustion

dx.doi.org/10.1021/sc300177j | ACS Sustainable Chem. Eng. 2013, 1, 364–373

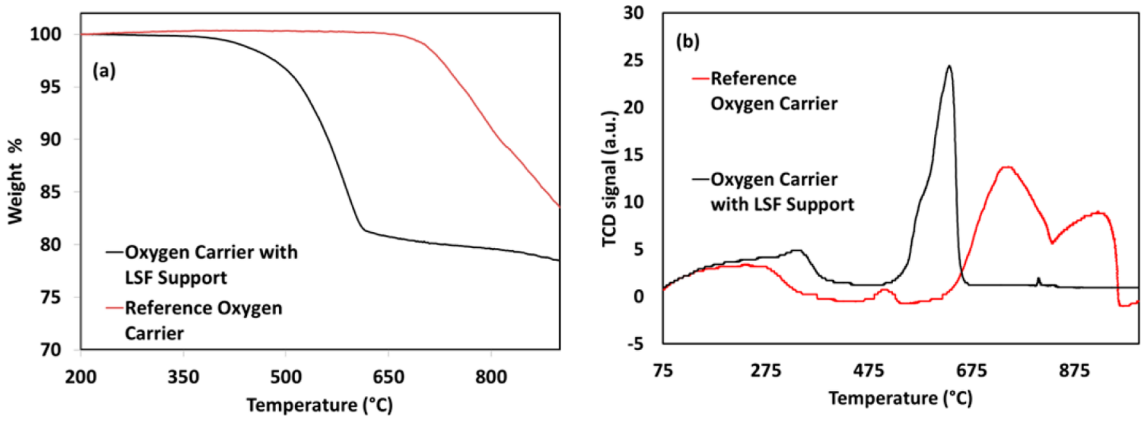

Figure 3. Initial temperature for reduction of Fe_2O_3-supported on LSF and TiO_2 in TGA (a) and H_2−TPR (b).

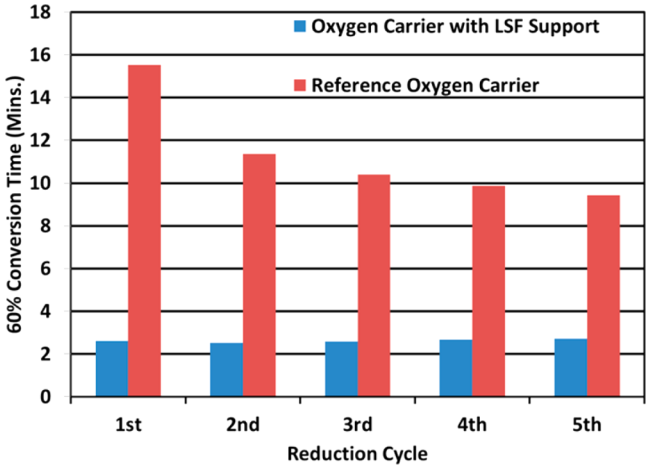

Figure 4. Time to achieve 60% conversion over the first five cycles using 10% H_2.

or gasification operations because the oxygen carrier will be in the form of Fe_3O_4/FeO prior to combustion.[10]

XRD analysis is performed to investigate the phase stability of the oxygen carrier. Figure 6 compares the dominant phases at the first reduction and oxidation as well as the 51st reduction and oxidation. The sizes of the key crystalline phases are listed in Table 2. The crystalline sizes are estimated using the Williamson−Hall method. A significant change in crystalline size is observed during the first redox cycle, which can be attributed to the solid-state reactions promoted by the redox reaction, leading to the stabilization of the crystalline phases. In fact, a noticeable amount of strontium ferrite phase coexists with perovskite and iron oxide phases in the fresh oxygen carrier, resulting from the incomplete solid-state reaction during the sample preparation/annealing step. This phase impurity is almost completely incorporated to the LSF structure after the first redox cycle (Figure 6). Table 2 also indicates that the crystalline sizes within the oxygen carrier remained relatively stable from the first redox cycle onward. This confirms the observations of insignificant sintering and oxygen carrier deactivation. XRD analysis on the Al_2O_3- and YSZ-supported samples show two primary phases: Fe_2O_3 and the support phase (ESI in Figure S7, Supporting Information).

Reaction with Gaseous Carbonaceous Fuels. An important feature of the chemical looping strategy is its ability for carbonaceous fuel conversion with in situ CO_2 capture. Syngas and natural gas are among the most investigated gaseous carbonaceous fuels in chemical looping applications. This section reports the conversion of CO and CH_4. CO is a major component in syngas besides H_2, whereas CH_4 is a key component of natural gas. The reactivity comparisons of the LSF-supported and TiO_2-supported oxygen carriers are shown in Figure 7. In terms of initial reaction rate with CO, Figure 7 indicates that the LSF-supported oxygen carrier is an order of magnitude more reactive than the reference, TiO_2-supported oxygen carrier. The LSF-enhanced oxygen carrier is approximately 40 times faster for achieving 33% conversion when CO

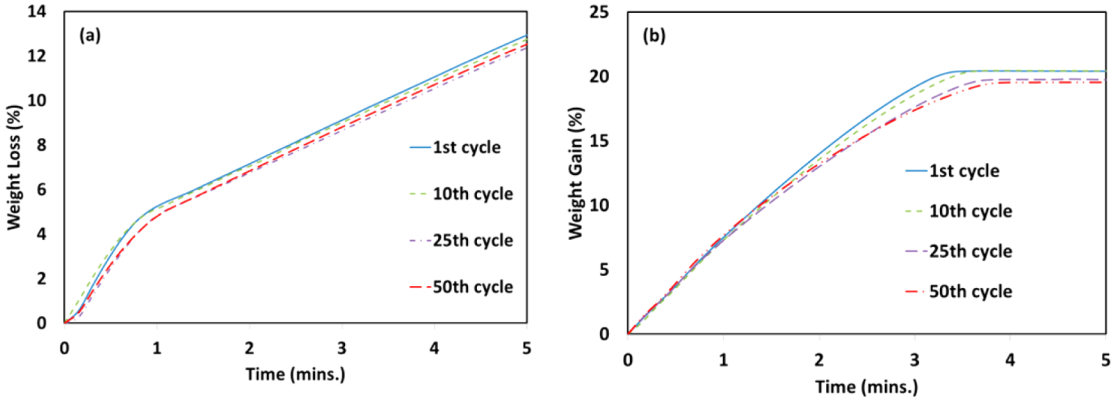

Figure 5. Cyclic redox experiment of (a) $La_{0.8}Sr_{0.2}FeO_{3-\delta}$-supported Fe_2O_3 in reduction cycles and (b) $La_{0.8}Sr_{0.2}FeO_{3-\delta}$-supported Fe_2O_3 in oxidation cycles. Reducing gas, 10% hydrogen; temperature, 900 °C; oxidizing gas, 10% oxygen; temperature, 900 °C.

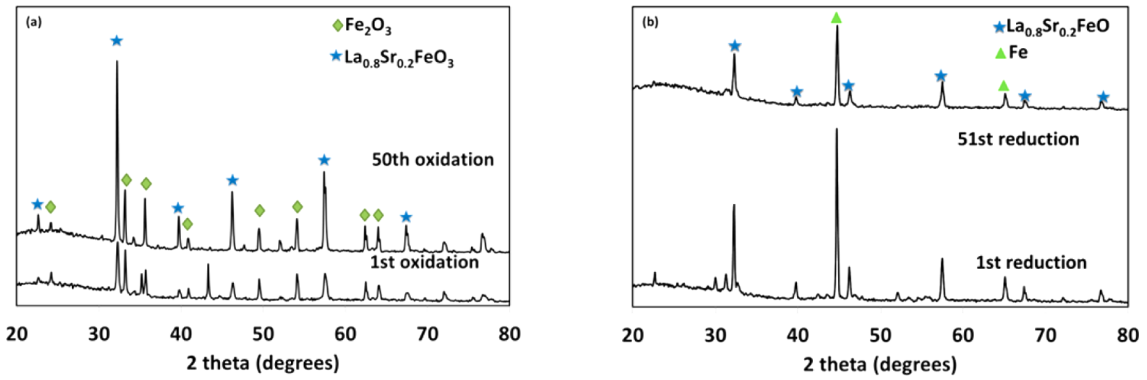

Figure 6. XRD spectra of LSF-supported Fe_2O_3 in oxidized (a) and reduced (b) forms over 51 reduction−oxidation cycles. Small unlabeled peaks in 1st cycle samples can be attributed to the insignificant amount of unconverted strontium ferrite from solid-state reactions.

Table 2. Crystalline Size Change during Multi-Cyclic Redox Reactions of LSF-Supported Fe_2O_3

	crystalline size in fresh oxygen carrier (Å)	crystalline size after 1st oxidation (Å)	crystalline size after 50th oxidation (Å)
Fe_2O_3	420	505	421
$La_{0.8}Sr_{0.2}FeO_3$	327	662	582

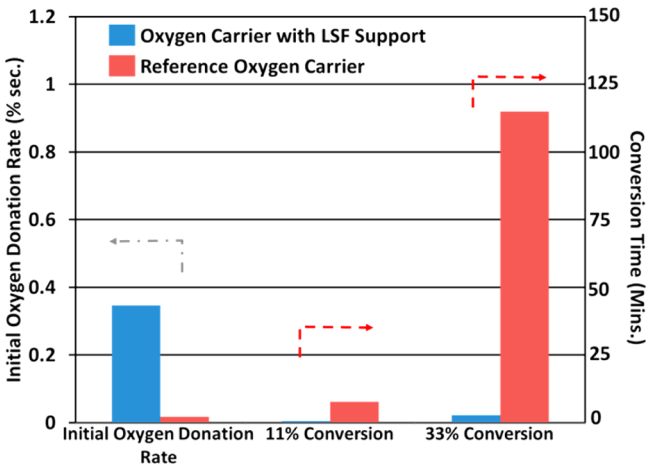

Figure 7. Reactivity comparisons of the reference and LSF- supported oxygen carriers in 10% CO at 900 °C.

is used as the fuel. An even more significant contrast is observed in terms of the oxygen carrier reactivity for CH_4 conversion, as shown in Figure 8. For comparison purpose, the CH_4 oxidation activities of YSZ- and Al_2O_3-supported oxygen carriers are also included in Figure 8. Although the formation of mixed Fe−Al oxides were reported to reduce the activity of Al_2O_3-supported Fe_2O_3 in some previous studies, XRD analysis in the current study indicates distinct support and iron oxide phases for both Al_2O_3- and YSZ-supported Fe_2O_3 (Figure S7, Supporting Information). Thus, the formation of a mixed metal oxide is insignificant. In terms of the initial rate for CH_4 oxidation, the LSF-supported oxygen carrier is approximately 8 times higher than the reference material, 2 times higher than the Al_2O_3-supported oxygen carrier, and 3.5 times higher than the YSZ-supported oxygen carrier. The LSF-enhanced oxygen carrier is 64 times faster to achieve 11% conversion than the reference material, 9 times faster than the Al_2O_3-supported oxygen carrier, 54 times faster than the YSZ-supported oxygen carrier, and 79 times faster than pure Fe_2O_3. A more pronounced reactivity disparity is observed for the oxygen carrier conversion at above 11%. In fact, the TiO_2- and YSZ-supported iron oxide as well as pure iron oxide did not reach 33% conversion during the 45 min (shown in gray in Figure 8) testing period. The Al_2O_3-supported sample achieved only 45% conversion within the 45 min reduction period. In contrast, the LSF-supported oxygen carrier is able to reach 100% conversion within a short duration. Although the excellent CH_4 conversion activity of the LSF-supported oxygen carrier may partially result

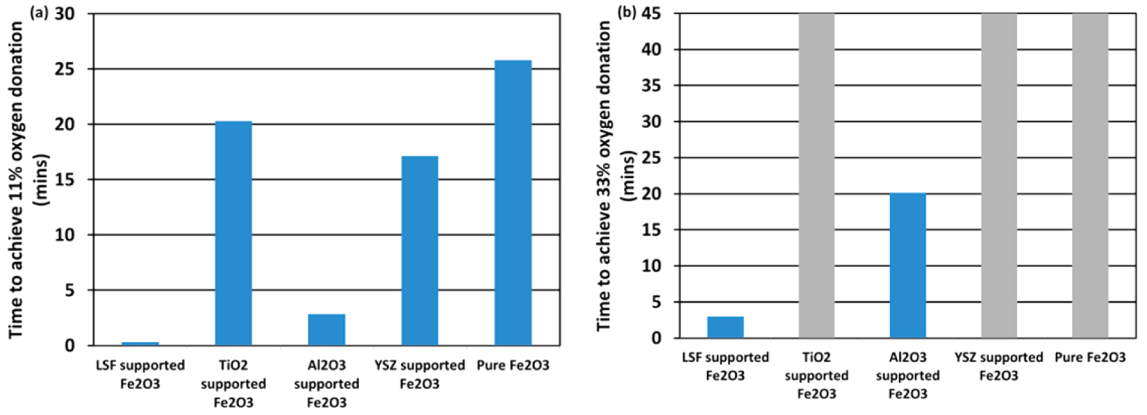

Figure 8. Reactivity comparisons of synthesized oxygen carriers in 10% CH_4 showing (a) time to achieve 11% conversion and (b) time to achieve 33% conversion.

dx.doi.org/10.1021/sc300177j | ACS Sustainable Chem. Eng. 2013, 1, 364−373

from the surface catalytic activity of the perovskite (LSF) support, the main contributor should be the mixed conductivity of LSF considering the relatively large crystallite sizes of both iron oxide and LSF support (Table 2). Unlike typical methane combustion/gasification reactions, gaseous oxygen is not used in chemical looping combustion of methane. Therefore, transfer of active O^{2-} from the solid primary oxide lattice to the oxygen carrier surface is likely to be the rate limiting step for methane oxidation. The ability of LSF to shuttle O^{2-} and electrons at a high conductivity allows effective combustion of methane and other fuels. The importance of mixed conductivity is further confirmed by the high activity of the LSF-supported oxygen carrier at low surface area. For instance, the LSF-supported oxygen carrier sintered for 28 h shows slightly higher activity when compared to the oxygen carrier sintered for 8 h (Figure S3, Supporting Information). Therefore, a low surface area did not adversely affect the activity of the oxygen carrier. The likely reason for a slightly higher activity is the more complete solid-tate reaction for the formation of more homogeneous LSF phase. It is also worthwhile to point out that although YSZ is a good O^{2-} conductor, it is a poor electronic conductor and thus cannot shuttle O^{2-} to and from the primary iron oxide. This explains the poor activity of YSZ when compared to a LSF-supported oxygen carrier even though both YSZ and LSF are O^{2-} conductive materials.

Besides being active for carbonaceous fuel conversion, an effective oxygen carrier should also be resistant toward coke formation, which may occur from a number of side reactions including the Boudouard reaction, methane decomposition, etc.[1,10,35] Coke formation data after 2 h of reaction between CO and oxygen carriers are listed in Table 3. As shown, the LSF-supported oxygen carrier is highly resistant toward coking formation through the Boudouard reaction. Merely 600 ppm (by weight) of carbon is observed after the 2 h reaction with the completely reduced oxygen carrier. In many previous studies, significant carbon deposition tends to occur upon near complete reduction of the oxygen carrier because reduced metal tends to catalyze the Boudouard reaction.[10,35] A lower carbon formation is observed for the TiO_2-supported oxygen carrier because it is only reduced by 45% after the 2 h duration. The good resistance toward carbon formation is likely to result from the mixed conductive support that provides high mobility lattice oxygen for in situ coke removal. In contrast to the insignificant coke formation observed when reacting with CO, significant coke formation (nearly 20% by weight) is identified on the LSF-supported oxygen carrier when CH_4 is used as the fuel in a 2 h reduction experiment. In order to investigate carbon deposition during the reduction stage, the LSF-supported oxygen carrier is reacted with CH_4 for 20 min prior to carbon analysis. The 20 min reduction time allows 100% oxygen carrier reduction while avoiding overexposure of the fully reduced oxygen carrier to CH_4. The coke content in the resultant solid sample is merely 400 ppm by weight. This indicates that significant coke formation in CH_4 conversion only takes place after complete depletion of active oxygen in the oxygen carrier. From a thermodynamics standpoint, the active oxygen in the oxygen carrier retards coke formation. Therefore, depletion of the same will favor coke formation on the oxygen carrier. In addition, transition metals including iron, which is formed upon reduction, can catalyze methane decomposition reactions. The fact that insignificant coke deposition occurred before 100% oxygen carrier reduction indicates that the LSF-supported oxygen carrier can be suitable for chemical looping applications. Prior studies have indicated that the maximum oxygen carrier conversion for an iron oxide-based oxygen carrier in a practical chemical looping process is limited to around 50%.[36] In fact, a low conversion of less than 11% (based on the current definition) is often maintained in the chemical looping combustion processes.[1] The low oxygen carrier conversion in actual chemical looping processes is likely to completely retard coke formation on the LSF-supported oxygen carrier. It is noted that the TiO_2-supported oxygen carrier exhibits low (0.3% by weight) coke formation after 2 h reaction with CH_4; this is attributed to slow reduction kinetics.

Table 3. Carbon Deposition Results When Using CO and CH_4 as Reducing Gases

material	reduced for 2 h in 10% CO (wt %)	reduced for 2 h in 10% CH_4 (wt %)	reduced for 20 min in 10% CH_4 (wt %)
Fe_2O_3 supported on $La_{0.8}Sr_{0.2}FeO_3$	0.06	19.40	0.04
Fe_2O_3 supported on TiO_2	0.02	0.31	0.02

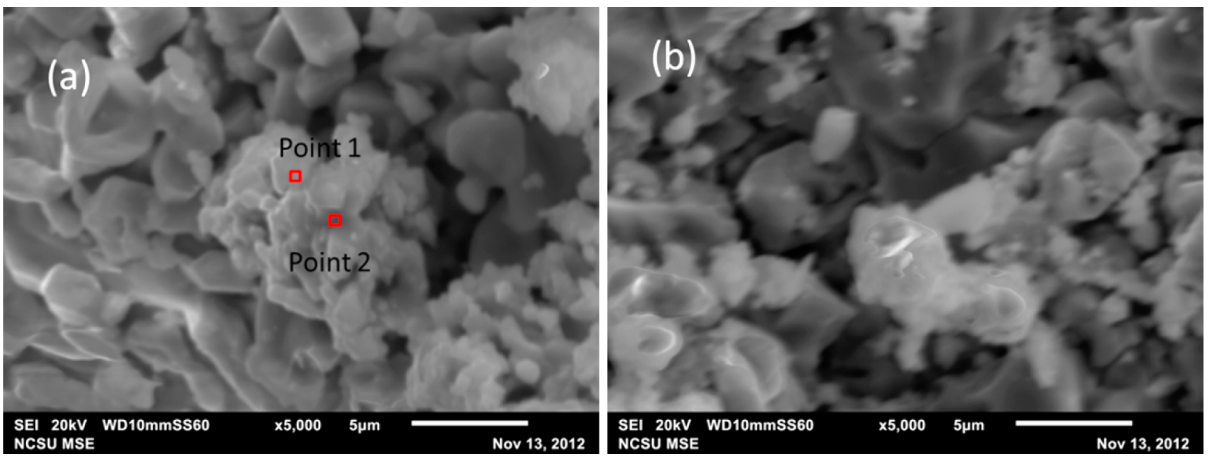

Figure 9. SEM image (20 kV) of LSF-supported Fe_2O_3 of (a) fresh particles and (b) after 51 oxidations and two locations where EDX point analyses are performed.

In fact, the TiO_2-supported oxygen carrier is only reduced by 25% after a 2 h duration. Regeneration of the reduced oxygen carrier is also performed. Coke formed on the LSF-supported oxygen carriers is found to be completely removed from the regeneration step.

Morphology Studies and Reaction Scheme. To obtain further understanding of the potential effect of the LSF-supported oxygen carrier, the oxygen carrier samples are characterized using a number of approaches including SEM/EDX, XRD, and XPS. As revealed by XRD analysis (Table 2 and Figure 6), the primary phases in oxidized oxygen carriers are Fe_2O_3 and LSF with crystalline sizes of around 50 nm. SEM images of the oxygen carriers as well as EDX spectra of several sample locations are illustrated in Figure 9 and Table 4.

Table 4. EDX Results of the LSF-Supported Oxygen Carrier at Points Represented in Figure 8(b) Taken at 10.0 kV for Enhanced Special Resolution

	point 1 (atomic %)	point 2 (atomic %)
O	64.3	54.52
Fe	27.2	41.14
La	6.1	1.71
Sr	2.3	2.63

Aluminum and carbon in the EDX spectra results from impurities introduced during the sample preparation stage in which a powder form of the LSF-supported Fe_2O_3 is spread across a piece of carbon tape placed on an aluminum sample holder. The SEM images indicate that the oxygen carrier is composed of dense grains of roughly 1−2 μm. At an accelerating voltage of 10 kV (special resolutions of ~0.5 μm), the elemental compositions obtained by EDX analysis at the various sample locations do not exhibit the presence of either pure LSF or Fe_2O_3 even though local enrichments of either LSF or Fe_2O_3 are identified (Table 4). The EDX line scan of La, Sr, and Fe reveal continuous distribution of these elements (Figure S6, Supporting Information). We also observed some deviation from the stoichiometric La:Sr ratio at selected locations in the fresh sample. This is in accordance with the presence of strontium ferrite observed under XRD, which leads to local enrichment of Sr compared to La. The strontium ferrite phase is fractionated into perovskite and ferrite phases after the first redox cycle. On the basis of the XRD and SEM/EDX results, it can be concluded that the Fe_2O_3 crystallites are finely divided by LSF at nanoscale. XPS analysis is carried out to characterize the surface composition of the oxygen carrier. The XPS spectra of the LSF-supported oxygen carrier surface is shown in Figure 10. The corresponding elemental composition of the surface is provided in Table 5. As indicated in Table 5, compared to the bulk LSF and Fe_2O_3 compositions, the oxygen carrier surface is enriched with LSF by approximately 45%. The surface enrichment of LSF is desired because it reduces the surface exposure of Fe_2O_3, which undergoes structural and phase changes over the redox cycles. Encapsulation of Fe_2O_3 can potentially lead to enhanced structural stability of the oxygen carrier. Although the mechanism for surface enrichment of LSF is subject to further studies, the high surface LSF concentration indicates that the redox reactions are likely to occur on the LSF surface, which provides active lattice oxygen conducted from the bulk phase. It is also noted that the oxygen concentration on the surface is slightly higher than that in the bulk. This indicates that the

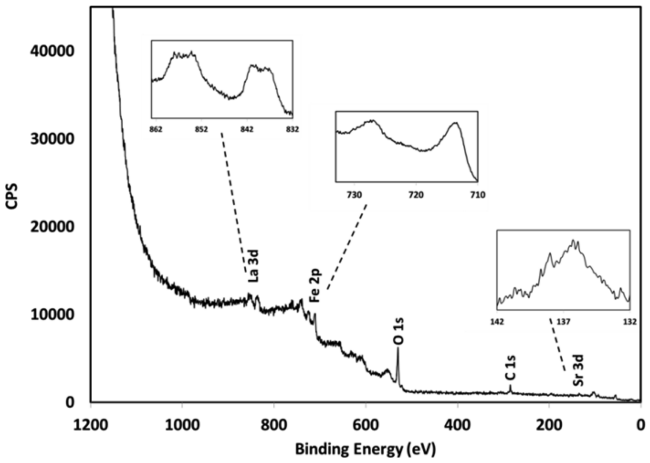

Figure 10. Surface composition analysis using XPS of the Fe_2O_3-supported on $La_{0.8}Sr_{0.2}FeO_3$.

Table 5. Elemental Composition Comparison of Fe_2O_3 Supported on LSF Oxygen Carrier of Bulk Compared to Surface[a]

	bulk atomic composition (%)	surface atomic composition (%)
O	60.00	72.83
Fe	33.72	19.35
La	5.03	6.39
Sr	1.25	1.42

[a]Carbon content in the XPS result is removed because it is introduced for binding energy calibration.

preferred termination surface is likely to contain a higher oxygen concentration. The result is consistent with the density functional theory (DFT) calculations performed by Mastrikov et al on relevant perovskites.[37]

On the basis of the morphology of the oxygen carrier, a reaction scheme for the redox reaction of the oxygen carrier is illustrated in Figure 11. As shown, the unique oxygen carrier is composed of nanoscale crystallites of (i) iron oxide as primary oxygen carrying material for lattice oxygen (O^{2-}) storage and (ii) LSF as MIEC support that facilities O^{2-} and electron/hole conduction. To participate in the fuel oxidation reactions, active O^{2-} is shuttled from the primary oxide to the oxygen carrier

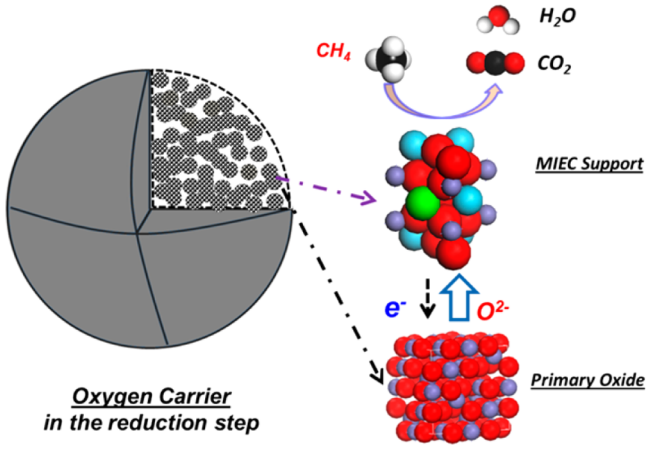

Figure 11. Proposed reduction reaction scheme of the LSF-supported Fe_2O_3 oxygen carrier.

dx.doi.org/10.1021/sc300177j | ACS Sustainable Chem. Eng. 2013, 1, 364−373

surface through the support. In the meantime, the electrons released by O^{2-} on the surface are conducted back to the primary oxide to maintain charge balance and to facilitate primary oxide reduction. With the primary oxide providing the O^{2-} and driving force (μ_{O2}) for the oxygen conduction in nanocrystallites of MIEC, each redox catalyst particle can be considered as a large collection of MIEC membrane reactors at nanoscale.[4] Although Fe_2O_3 is not a good conductor for both electrons and oxygen anions, the very small length scale for O^{2-} diffusion in the Fe_2O_3 nanocrystallites ensures easy accessibility of oxygen. As confirmed by the experimental results, nearly 100% of the O^{2-} stored in the primary oxide is accessible to the redox reactions. Compared to conventional MIEC membrane reactors, the redox catalyst can be more robust and flexible because a dense membrane layer is unnecessary. The above-mentioned mechanism is consistent with the authors' previous DFT and experimental studies on supported oxygen carriers.[23,24]

CONCLUSIONS

The present study investigates the use of mixed conductive support such as lanthanum strontium ferrite (LSF) to enhance the performance of iron-based oxygen carriers. Using a simple solid-state synthesis method, oxygen carriers composed of interpenetrated nanocrystallites of iron oxide and LSF support are obtained. The LSF enhanced oxygen carrier exhibits more than an order of magnitude higher reactivity when compared to a reference, TiO_2-supported oxygen carrier as well as Al_2O_3- and YSZ-supported oxygen carriers. The mix-conductive support enhanced oxygen carrier also becomes active for redox reactions at a much lower temperature. In addition, the improved oxygen carrier shows excellent recyclability and good resistance toward coke formation for CO and CH_4 conversion. The significantly enhanced redox performance of the LSF-supported oxygen carrier is likely to result from the facile lattice oxygen and electron/hole pathways created by the mixed conductive support. To be more specific, the mixed conductive support enables fast solid state O^{2-} and electron/hole exchange between the iron oxide nanocrystallites and the oxygen carrier particle surface, thereby allowing effective oxygen removal and restoration of the oxygen carrier during the redox reactions while maintaining charge balance within the oxygen carrier. By embedding and stabilizing iron oxide nanocrystallites of less than 100 μm in a matrix of nanosized mixed conductive support, all active lattice oxygen within the iron oxide are made accessible for fast redox reactions via solid state conduction. The findings from the present research can lead to a potentially effective approach for rational optimization of oxygen carriers for chemical looping applications. These findings indicate that the incorporation of mixed conductive and structurally compatible support with an oxygen-carrying primary metal oxide can lead to high performance oxygen carriers with good reactivity, robustness, and sintering resistance. The resulting oxygen carrier particle can be considered as an ensemble of nanoscale mixed conductive membrane reactors in which the primary metal oxide is used as the oxygen source or sink in the redox reactions of the chemical looping process.

ASSOCIATED CONTENT

Supporting Information

Additional information regarding synthesis and characterization procedures and results. This material is available free of charge via the Internet at http://pubs.acs.org.

AUTHOR INFORMATION

Corresponding Author

*E-mail: Fli5@ncsu.edu.

Notes

The authors declare no competing financial interest.

ACKNOWLEDGMENTS

This work was supported by the North Carolina State University Start-Up Fund. We acknowledge Feng He and Kit Yeung in the setup of the experimental apparatus.

REFERENCES

(1) Adanez, J.; Abad, A.; Garcia-Labiano, F.; Gayan, P.; de Diego, L. F. Progress in chemical-looping combustion and reforming technologies. *Prog. Energy Combust.Sci.* **2012**, *38*, 215−282.

(2) Shah, K.; Moghtaderi, B.; Wall, T. Selection of suitable oxygen carriers for chemical looping air separation: A thermodynamic approach. *Energy Fuel.* **2012**, *26*, 2038−2045.

(3) Hossain, M. M.; de Lasa, H. I. Chemical-looping combustion (CLC) for inherent separations—A review. *Chem. Eng. Sci.* **2008**, *63*, 4433−4451.

(4) Thursfield, A.; Murugan, A.; Franca, R.; Metcalfe, I. S. Chemical looping and oxygen permeable ceramic membranes for hydrogen production − A review. *Energy Environ. Sci.* **2012**, *5*, 7421−7459.

(5) Li, F.; Fan, L.-S. Clean coal conversion processes − Progress and challenges. *Energy Environ. Sci.* **2008**, *1*, 248.

(6) Ishida, M.; Jin, H. A new advanced power-generation system using chemical-looping combustion. *Energy* **1994**, *19*, 415−422.

(7) Kang, K.-S.; Kim, C.-H.; Bae, K.-K.; Cho, W.-C.; Kim, S.-H.; Park, C.-S. Oxygen-carrier selection and thermal analysis of the chemical-looping process for hydrogen production. *Int. J. Hydrogen Energy* **2010**, *35*, 12246−12254.

(8) Ishida, M.; Jin, H. CO2 recovery in a power plant with chemical looping combustion. *Energy Convers. Manage.* **1997**, *38* (Supplement), S187−S192.

(9) Lyngfelt, A. Oxygen carriers for chemical looping combustion − 4000 h of operational experience. *Oil Gas Sci. Technol.* **2011**, *66*, 161−172.

(10) Fan, L.-S. *Chemical Looping Systems for Fossil Energy Conversions*; John Wiley & Sons, Inc.: New York, 2010.

(11) Svoboda, K.; Slowinski, G.; Rogut, J.; Baxter, D. Thermodynamic possibilities and constraints for pure hydrogen production by iron based chemical looping process at lower temperatures. *Energy Convers. Manage.* **2007**, *48*, 3063−3073.

(12) Adánez, J.; de Diego, L. F.; García-Labiano, F.; Gayán, P.; Abad, A.; Palacios, J. M. Selection of oxygen carriers for chemical-looping combustion. *Energy Fuel.* **2004**, *18*, 371−377.

(13) Lyngfelt, A.; Johansson, M.; Mattisson, T. Chemical-Looping Combustion − Status of Development. In *Proceedings of the 9th International Conference on Circulating Fluidized Beds*; Hamburg, Germany, 2008.

(14) Rydén, M.; Johansson, M.; Lyngfelt, A.; Mattisson, T. NiO supported on Mg−ZrO_2 as oxygen carrier for chemical-looping combustion and chemical-looping reforming. *Energy Environ. Sci.* **2009**, *2*, 970.

(15) Li, F.; Kim, H. R.; Sridhar, D.; Wang, F.; Zeng, L.; Chen, J.; Fan, L.-S. Syngas Chemical Looping gasification process: Oxygen carrier particle selection and performance. *Energy Fuel* **2009**, *23*, 4182−4189.

(16) Rydén, M.; Lyngfelt, A.; Mattisson, T.; Chen, D.; Holmen, A.; Bjørgum, E. Novel oxygen-carrier materials for chemical-looping combustion and chemical-looping reforming; $LaxSr_{1-x}FeyCo_{1-y}O_3-\delta$ perovskites and mixed-metal oxides of NiO, Fe_2O_3 and Mn_3O_4. *Int. J. Greenhouse Gas Control* **2008**, *2*, 21−36.

(17) Murugan, A.; Thursfield, A.; Metcalfe, I. S. A chemical looping process for hydrogen production using iron-containing perovskites. *Energy Environ. Sci.* **2011**, *4*, 4639.

(18) Sarshar, Z.; Kleitz, F.; Kaliaguine, S. Novel oxygen carriers for chemical looping combustion: $La_{1-x}Ce_xBO_3$ (B = Co, Mn) perovskites synthesized by reactive grinding and nanocasting. *Energy Environ. Sci.* **2011**, *4*, 4258.
(19) Azimi, G.; Rydén, M.; Leion, H.; Mattisson, T.; Lyngfelt, A. $(MnzFe_{1-z})_yO_x$ combined oxides as oxygen carrier for chemical-looping with oxygen uncoupling. *AIChE J.* **2012**, n/a−n/a.
(20) Fan, L.-S.; Zeng, L.; Wang, W.; Luo, S. Chemical looping processes for CO_2 capture and carbonaceous fuel conversion − Prospect and opportunity. *Energy Environ. Sci.* **2012**, *5*, 7254.
(21) Bouwmeester, H. J. M. Dense ceramic membranes for methane conversion. *Catal. Today* **2003**, *82*, 141−150.
(22) Zhang, K.; Sunarso, J.; Shao, Z.; Zhou, W.; Sun, C.; Wang, S.; Liu, S. Research progress and materials selection guidelines on mixed conducting perovskite-type ceramic membranes for oxygen production. *RSC Adv.* **2011**, *1*, 1661−1676.
(23) Li, F.; Luo, S.; Sun, Z.; Bao, X.; Fan, L.-S. Role of metal oxide support in redox reactions of iron oxide for chemical looping applications: Experiments and density functional theory calculations. *Energy Environ. Sci.* **2011**, *4*, 3661.
(24) Li, F.; Sun, Z.; Luo, S.; Fan, L.-S. Ionic diffusion in the oxidation of iron—Effect of support and its implications to chemical looping applications. *Energy Environ. Sci.* **2011**, *4*, 876.
(25) Mattisson, T.; Lyngfelt, A.; Cho, P. The use of iron oxide as an oxygen carrier in chemical-looping combustion of methane with inherent separation of CO_2. *Fuel* **2001**, *80*, 1953−1962.
(26) Corbella, B. M.; Palacios, J. M. Titania-supported iron oxide as oxygen carrier for chemical-looping combustion of methane. *Fuel* **2007**, *86*, 113−122.
(27) Jerndal, E.; Leion, H.; Axelsson, L.; Ekvall, T.; Hedberg, M.; Johansson, K.; Källén, M.; Svensson, R.; Mattisson, T.; Lyngfelt, A. Using low-cost iron-based materials as oxygen carriers for chemical looping combustion. *Oil Gas Sci. Technol.* **2011**, *66*, 235−248.
(28) Leion, H.; Mattisson, T.; Lyngfelt, A. Use of ores and industrial products as oxygen carriers in chemical-looping combustion. *Energy Fuel.* **2009**, *23*, 2307−2315.
(29) Mattisson, T.; Johansson, M.; Lyngfelt, A. Multicycle reduction and oxidation of different types of iron oxide particlesapplication to chemical-looping combustion. *Energy Fuel.* **2004**, *18*, 628−637.
(30) Roux, S.; Bensakhria, A.; Antonini, G. Study and improvement of the regeneration of metallic oxides used as oxygen carriers for a new combustion process. *Int. J. Chem. React. Eng.***2006**, *4*.
(31) Adanez, J.; García-Labiano, F.; de Diego, L. F.; Gayán, P.; Celaya, J.; Abad, A. Characterization of Oxygen Carriers for Chemical-Looping Combustion. In *Greenhouse Gas Control Technologies 7*; Elsevier Science Ltd: Oxford, 2005; pp 105−113.
(32) Kolbitsch, P.; Pröll, T.; Hofbauer, H. Modeling of a 120 kW chemical looping combustion reactor system using a Ni-based oxygen carrier. *Chem. Eng. Sci.* **2009**, *64*, 99−108.
(33) Pröll, T.; Mayer, K.; Bolhàr-Nordenkampf, J.; Kolbitsch, P.; Mattisson, T.; Lyngfelt, A.; Hofbauer, H. Natural minerals as oxygen carriers for chemical looping combustion in a dual circulating fluidized bed system. *Energy Procedia* **2009**, *1*, 27−34.
(34) Zhao, Y.; Shadman, F. Reduction of ilmenite with hydrogen. *Ind. Eng. Chem. Res.* **1991**, *30*, 2080−2087.
(35) Rohmund, F.; Falk, L. K. L.; Campbell, E. E. B. Iron catalyzed growth of carbon nanotubes. *AIP Conf. Proc.* **2000**, *544*, 234−237.
(36) Li, F.; Zeng, L.; Velazquez-Vargas, L. G.; Yoscovits, Z.; Fan, L.-S. Syngas chemical looping gasification process: Bench-scale studies and reactor simulations. *AIChE J.* **2010**, *56*, 2186−2199.
(37) Mastrikov, Y. A.; Merkle, R.; Heifets, E.; Kotomin, E. A.; Maier, J. Pathways for oxygen incorporation in mixed conducting perovskites: A DFT-based mechanistic analysis for (La, Sr)$MnO_{3-\delta}$. *J. Phys. Chem. C* **2010**, *114*, 3017−3027.